nature communications

Article

https://doi.org/10.1038/s41467-024-53744-x

Heterochiral coupling to bilateral β-turn structured azapeptides bearing two remote chiral centers

Received: 27 June 2024

Accepted: 22 October 2024

Published online: 28 October 2024

Check for updates

Xiaosheng Yan[1,4], Jinlian Cao[1], Huan Luo[1], Zhao Li[1], Zexing Cao[2], Yirong Mo[3] & Yun-Bao Jiang[1]

Enantioselective synthesis governed by chiral catalysts has been extensively developed, but that without any chiral auxiliaries or chiral catalysts is rare, particularly when remote stereogenic centers are involved. Here we report an enantioselectivity of heterochiral coupling in the one-pot reaction of racemic hydrazides with achiral 1,4-bis(isothiocyanine)benzene, yielding preferentially the heterochiral bilateral azapeptides over the homochiral ones. Despite bearing two hydrogen-bonded β-turn structures that allow intramolecular chiral transfer, the bilateral azapeptide products have two chiral centers separated by 14 atoms or 15 bonds, which prevent the direct intramolecular asymmetric communication between the two chiral centers. Interestingly, the heterochiral azapeptides feature intermolecular hydrogen bonding stacking between homochiral β-turns to form a superstructure of alternative *M*- and *P*-helices in the crystals. In contrast, the homochiral azapeptide counterparts adopt a β-sheet-like structure, which is less favorable compared to the helical-like superstructure from heterochiral azapeptides, accounting for the favored heterochiral coupling of the one-pot reaction. This work demonstrates enantioselective synthesis involving distant chiral centers through the formation of biomimetic superstructures, opening up new possibilities for the regulation of enantioselectivity.

Enantioselective synthesis using chiral catalysts has undergone tremendous development[1–5]. However, enantioselective synthesis without additional chiral auxiliaries, which is critical for the understanding of biological homochirality[6–8], is relatively rare. Several examples have demonstrated the enantioselective fragment couplings for peptides in this context. For instance, the chemical synthesis of dipeptide from *N*-acyl α-amino acids and α-amino acid amides or esters showed a preference for heterochiral outcomes, which was attributed to the intramolecular steric hindrance between adjacent chiral centers[9,10]. Blackmond et al.[11] demonstrated heterochiral selectivity of thiol-catalyzed peptide ligation between amidonitriles and amino acids, amino amides, or peptides, offering a mechanism for both symmetry breaking and chiral amplification of the reactants and homochiral dipeptide products. Helical oligomers formed from L-C^{α}-methyl valine preferentially incorporate proteinogenic amino acids with D-configuration[12]. Lahav et al.[13–15] showed that antiparallel racemic β-sheets consisting of alternant oligo-L- and oligo-D-amino acid peptides function as intermediate templates to

[1]MOE Key Laboratory of Spectrochemical Analysis and Instrumentation, Department of Chemistry, College of Chemistry and Chemical Engineering, Xiamen University, Xiamen 361005, China. [2]State Key Laboratory of Physical Chemistry of Solid Surfaces, Department of Chemistry, College of Chemistry and Chemical Engineering, Xiamen University, Xiamen 361005, China. [3]Department of Nanoscience, Joint School of Nanoscience and Nanoengineering, University of North Carolina at Greensboro, Greensboro, NC 27401, USA. [4]Present address: School of Pharmaceutical Sciences, Xiamen University, Xiamen 361102, China. e-mail: ybjiang@xmu.edu.cn

drive homochiral coupling for oligopeptides. Ghadiri et al.[16–18] reported that an amphiphilic homochiral α-helical oligopeptide induces homochiral peptide coupling via the formation of homochiral supramolecular coiled-coil structure.

In the aforementioned examples, the outcomes have adjacent chiral centers that provide local stereogenic constraints. Achieving enantioselective coupling of remote chiral centers, however, is much more challenging[19–22]. Clayden et al.[23] demonstrated that helical peptides govern the enantioselective coupling in the absence of local chiral residues. In that example, the *N*- and *C*-terminal chiral centers are well separated by 14 atoms, but a consecutive intramolecular hydrogen bonding network establishes the asymmetric communication between the two chiral centers, directing the enantioselective coupling. Such helical peptides with a single remote chiral center can even serve as enantioselective organocatalysts for the conjugate addition reaction[24]. These structures nicely exemplified remote chiral communication despite being synthetically challenging. The works of Lahav et al.[13–15] and Ghadiri et al.[16–18] inspired us that the formation of chiral assembled structures, such as β-sheet and helical structures, could be an alternative means to achieve enantioselective coupling for remote chiral centers.

Here, we intend to create an enantioselective coupling that, without any chiral auxiliaries, involves two remote chiral centers through the formation of chiral assembled structures. We chose *N*-acylphenylalanine-based bilateral *N*-amidothioureas, i.e., bilateral azapeptides **AcFTU2** (L,L-, L,D-, D,D-), as candidates (Fig. 1a). **AcFTU2** has two intramolecular hydrogen-bonded β-turn structures[25,26], yet the two chiral centers are separated by 14 atoms (Fig. 1a). A more important feature is that the helical β-turn structures can form chiral assembled structures via intermolecular interactions[27–33], possibly driving enantioselective coupling during the synthesis of **AcFTU2** from the enantiomeric or racemic reactants. We did observe a preference for the heterochiral coupling in the one-pot reaction of racemic *N*-acylphenylalanine-based hydrazides with the achiral 1,4-di(isothiocyanine)benzene, yielding more heterochiral azapeptide L,D-**AcFTU2** than the statistical yield, over homochiral counterparts L,L- and D,D-**AcFTU2**. The heterochiral products exhibit helical-like superstructures. This is more favorable than the β-sheet-like organization from the homochiral counterparts, accounting for the favored heterochiral coupling of the one-pot reaction. As such, chiral amplification of the hydrazide starting material is achieved by treating it with achiral 1,4-di(isothiocyanine)benzene, which selectively takes a pair of the enantiomeric hydrazides.

Results

Heterochiral coupling to bilateral azapeptides

We designed a one-pot reaction of *N*-acylamino acid-based hydrazide, **$AcFN_2H_3$**, with achiral 1,4-di(isothiocyanine)benzene, **$Ph(NCS)_2$**, that leads to bis(*N*-amidothiourea), **AcFTU2**, in which two chiral residues are far away by 14 atoms or 15 bonds, with three possible diastereomers L,L-, D,D-, and L,D-**AcFTU2** whose statistical percentages would be 25%, 25%, and 50%, respectively (Fig. 1b).

Different from the theoretical statistical distributions of the coupling products, we observed a favored heterochirality in the reaction

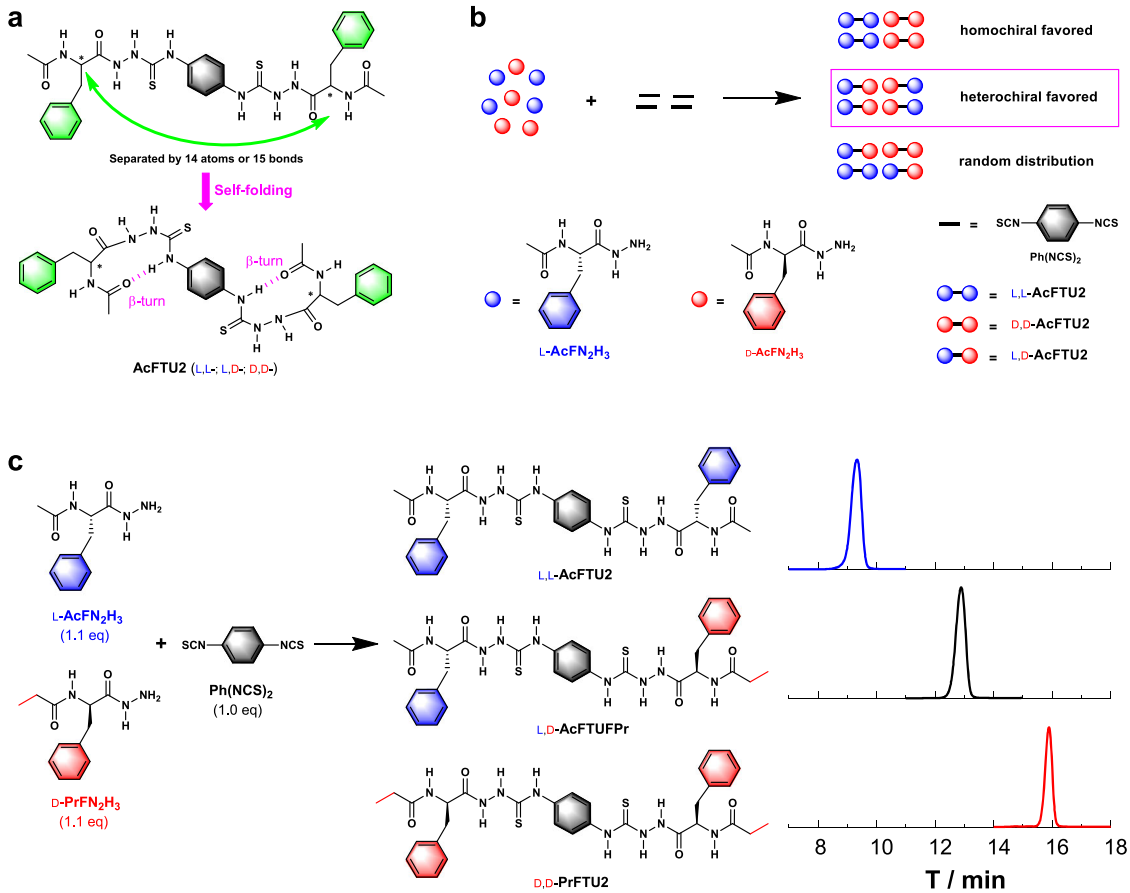

Fig. 1 | Design of the enantioselective bilateral couplings. a Structures of *N*-acylphenylalanine based bilateral azapeptides L,L-/L,D-/D,D-**AcFTU2**, containing two hydrogen-bonded β-turns. The asterisks in the structures indicate chiral carbons. **b** Schematic diagrams of three different fates for the bilateral reaction of L-/D-**$AcFN_2H_3$** with **$Ph(NCS)_2$**. **c** Reactions of L-**$AcFN_2H_3$** and D-**$PrFN_2H_3$** with **$Ph(NCS)_2$** and HPLC traces of the three products. Experimental conditions: L-**$AcFN_2H_3$** (0.22 mmol), D-**$PrFN_2H_3$** (0.22 mmol), and **$Ph(NCS)_2$** (0.2 mmol) in 10 mL solvent is stirred at set temperatures for 8 h.

Table 1 | Diastereoselectivity in the reaction of L-AcFN$_2$H$_3$ and D-PrFN$_2$H$_3$ with Ph(NCS)$_2$

Entry	Solvent	*T*, °C	Total yield, %[a]	% L,D-AcFTUFPr[b]	Precipitation
1	MeCN	25	>99	56	Yes
2	MeCN	50	>99	65	Yes
3	MeCN	80	>99	72	Yes
4	MeCN	100[c]	>99	84	Yes
5	MeOH	25	>99	58	Yes
6	MeOH	65	87	66	Yes
7	MeOH	100[c]	/	/	No
8	MeCN/H_2O[d]	80	95	62	Yes
9	MeCN/H_2O[d]	100[c]	5	/	Yes
10	DMF	25	>99	49	No
11	DMF	80	95	50	No
12	DMSO	25	>99	51	No
13	DMSO	80	>99	50	No
14	THF	25	>99	56	Yes
15	THF	65	>99	66	Yes
16	THF	100 [c]	/	/	No

[a]Determined by ^{1}H NMR (500 MHz).
[b]Determined by HPLC. The content of the heterochiral product is taken to describe the diastereoselectivity.
[c]Reaction is conducted in a high-pressure reactor (a 20-mL sealed hydrothermal reactor without applying external pressure).
[d]5 mL MeCN and 5 mL H_2O.

of *rac*-**AcFN$_2$H$_3$** (equal L- and D-**AcFN$_2$H$_3$**) with **Ph(NCS)$_2$**, yielding preferentially the L,D-bilateral azapeptide **AcFTU2,** *ca*. 74% when reacting in MeCN at 80 °C, a general condition for the synthesis of such bilateral azapeptides[27,28], which is evaluated from absorption spectral measurements (Supplementary Fig. 1). In real reaction systems, for a more facile measurement of the distribution of the products, we used D-**PrFN$_2$H$_3$**, instead of D-**AcFN$_2$H$_3$** (Fig. 1b), to form a quasi-racemate[13–15,34] with the same equivalent of acetylated L-**AcFN$_2$H$_3$**, enabling the HPLC analysis of the highly polar products (Fig. 1c). The hydrazides were added in 10% excess to ensure complete reactions.

Using MeCN as a solvent, the products precipitate gradually from the solution. At room temperature (25 °C), the heterochiral L,D-product is slightly favored over the homochiral ones (56:44), showing a weak heterochiral selectivity. Significantly, the heterochirality increases dramatically with increasing temperature, up to 84:16 at 100 °C (Table 1 and Supplementary Fig. 2). This means that in the one-pot reaction, when the first step takes place with L-hydrazide, the follow-up step is more likely takes the D-counterpart, despite that the two chiral centers are distant in the product molecule and separated by a central benzene ring.

In protic solvent MeOH, similar temperature-dependent diastereoselectivity was found in the distributions of the insoluble products (Table 1). However, no products were detected when the reaction was carried out in a high-pressure reactor at 100 °C. In 1:1 (v/v) MeCN/H_2O at 80 °C, the heterochiral selectivity is preserved partly as in pure MeCN, but at a higher temperature of 100 °C the yield drops sharply. Both of those suggest that protic solvents are not suitable for the heterochiral coupling reaction to proceed at high temperatures.

Using highly polar solvents dimethyl formamide (DMF) and DMSO in which no product precipitates, the heterochiral selectivity disappears, indicating that precipitation may play a role in the diastereoselective coupling. In aprotic solvent THF of medium polarity, preferred heterochirality is also found at a temperature at which insoluble products form, but at a higher temperature, such as 100 °C, the reaction is destroyed. In addition, solvents of low polarity are not suitable due to the limited solubility of the hydrazide reactant.

As the propionylated and acetylated reactants may exhibit different reactivity in the one-pot reaction, a control reaction of L-**AcFN$_2$H$_3$** and L-**PrFN$_2$H$_3$** with **Ph(NCS)$_2$** was carried out (Supplementary Fig. 3). No selectivity but a random distribution in the reaction products was found, indicating that the diastereoselectivity shown in Table 1 does not result from the possible difference in the reactivity of those two reactants. This is further supported by the comparable rate constants for the reaction of phenyl isothiocyanate, a mono-NCS analog of **Ph(NCS)$_2$**, with hydrazide L-**AcFN$_2$H$_3$** or D-**PrFN$_2$H$_3$** in MeCN (5.34×10^{-3} L mol^{-1} s^{-1} versus 5.42×10^{-3} L mol^{-1} s^{-1}, Supplementary Fig. 4).

The preferential heterochirality was also confirmed by the reaction rate constants of mono-reacted intermediate L-**AcFTUNCS** (Supplementary Fig. 5), which is fully soluble in the reaction solution, with hydrazides to yield L,L- and L,D-**AcFTU2** ($k_{L,L}$ and $k_{L,D}$), respectively (Fig. 2a). We measured $k_{L,L}$ and $k_{L,D}$ in MeCN over the temperature range of 25–80 °C. Data show that $k_{L,D}$ is higher than $k_{L,L}$ (Fig. 2b and Supplementary Table 1). More importantly, the ratio of reaction rate constants, $k_{L,D}/(k_{L,L} + k_{L,D})$, increases with temperature, which is consistent with the temperature dependence of heterochiral selectivity in MeCN (Supplementary Fig. 6).

β-Turns and intramolecular chiral transfer

To get insight into the driving forces for the preferred heterochiral coupling, we first investigated the structural characteristics of L,D- and L,L-**AcFTU2** by examining their crystal structures. Slow diffusion of diethyl ether vapor into DMF solutions of L,D- and L,L-**AcFTU2** in sealed wide-mouthed bottles for 3–4 days leads to crystals suitable for X-ray crystal structure analyses (for crystallographic data, see Supplementary Table 2). Crystal structure of heterochiral L,D-**AcFTU2** (Fig. 3a) exhibits a type II (**β1**, containing L-phenylalanine residue) and a type II′ (**β1′**, containing D-phenylalanine residue) β-turn structures referring to the torsion angles (Supplementary Table 3)[35,36], maintained respectively by two intramolecular ten-membered ring N–H^d•••^{e}O=C hydrogen bonds. The homochiral counterpart L,L-**AcFTU2** (Fig. 3b) contains a type II β-turn structure at each side of the molecule (labeled as **β2** and **β3**), but with different parameters (Supplementary Table 3). Absorption and CD spectra of L,L- and D,D-**AcFTU2** in MeCN show exciton-coupled characteristic at 268 and 282 nm, indicating an intramolecular coupling of phenylalanine residue, phenyl thiourea and *p*-phenylenediamine chromophores[37], likely mediated by the β-turn structures in them that afford the intramolecular chirality transfer (Supplementary Figs. 7 and Fig. 3c). The mesomeric L,D-**AcFTU2** displays the same absorption spectrum as L,L- and D,D-**AcFTU2**, but it is CD silent (Fig. 3c). Solvent accessibilities and temperature coefficients of the chemical shifts of the –NH protons in DMSO-d_6/CD_3CN binary solvents verify the existence of β-turn structures involving –NH^d proton in the intramolecular hydrogen bonds in solutions (Supplementary Figs. 8 and 9)[38,39]. For example, the temperature coefficients of –NH^d proton, −3.48 ppb/°C for L,L-**AcFTU2,** and −3.51 ppb/°C for L,D-**AcFTU2** (Fig. 3d), are much lower than those of the rest three -NH protons.

The two chiral centers in **AcFTU2** are far separated by 14 atoms or 15 bonds, and the central benzene ring may, to some extent, disturb the intramolecular hydrogen bonding network (Fig. 3a, b), thereby direct intramolecular asymmetric communication between the two chiral centers might be weakened. This is supported by the comparable intramolecular hydrogen bonds that maintain the β-turns in L,D- and L,L-**AcFTU2** monomers, deduced from the profiles of the solvent composition and temperature-dependent chemical shifts of –NH^d protons involved in the β-turns that are almost overlapped (Supplementary Figs. 10 and Fig. 3d), as well as the close stabilizing energies at optimal geometries (Supplementary Fig. 11).

https://doi.org/10.1038/s41467-024-53744-x

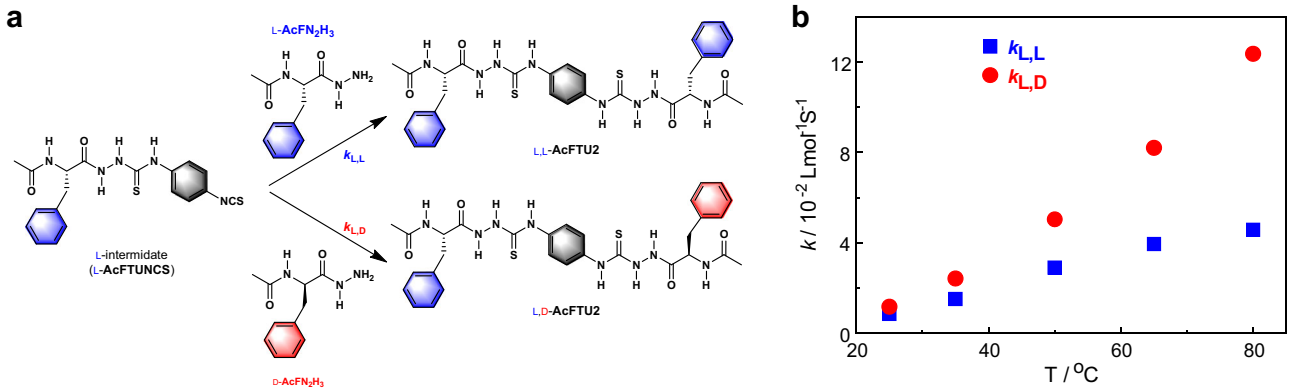

Fig. 2 | Reaction rate constants. a The reactions between L-intermediate (L-**AcFTUNCS**) and L-**AcFN$_2$H$_3$** or D-**AcFN$_2$H$_3$**, yielding homochiral L,L-**AcFTU2** and heterochiral L,D-**AcFTU2**, respectively. **b** The reaction rate constants $k_{L,L}$ and $k_{L,D}$ in MeCN versus reaction temperature.

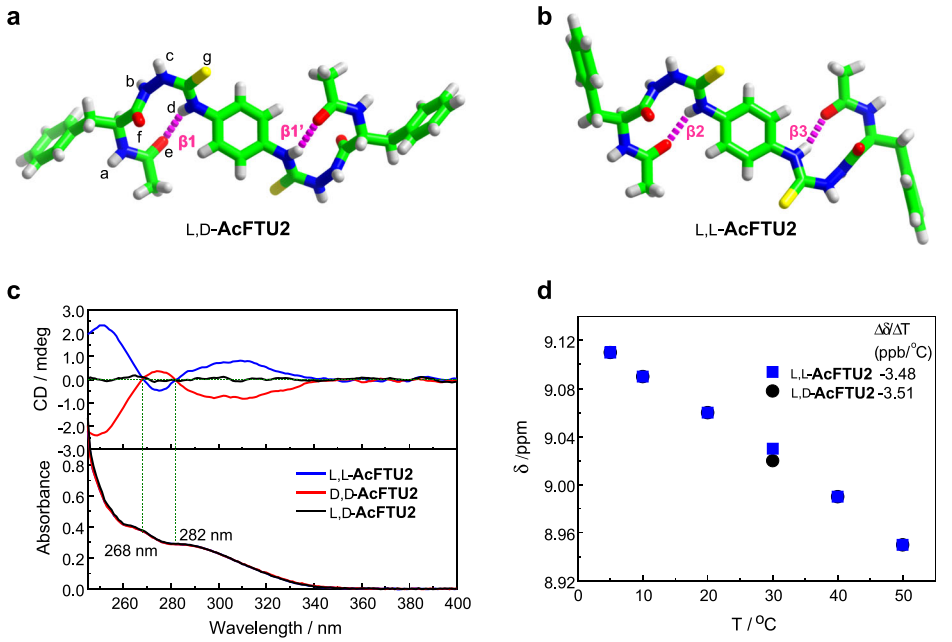

Fig. 3 | β-Turn structures. a X-ray crystal structure of L,D-**AcFTU2** with atom labeling. **b** X-ray crystal structure of L,L-**AcFTU2**. Intramolecular hydrogen bonds are shown by dashed pink lines and β-turn structures are labeled as **β1**, **β1'** for L,D-**AcFTU2**, and **β2** and **β3** for L,L-**AcFTU2**. **c** Absorption and CD spectra of L,L-**AcFTU2** (blue line), D,D-**AcFTU2** (red line), and L,D-**AcFTU2** (black line) in 99/1 (v/v) MeCN/DMSO. Concentration: 20 μM. **d** Temperature-dependent chemical shifts and the fitted temperature coefficients (Δδ/ΔT) of −NH^d protons of L,D-**AcFTU2** and L,L-**AcFTU2** in 95:5 (v/v) CD_3CN/DMSO-d_6 mixtures.

Absorption and CD spectra of hydrazide substrate L-**AcFN$_2$H$_3$** and mono-reacted intermediate L-**AcFTUNCS** were also recorded (Supplementary Fig. 12). In comparison to the CD spectrum of L-**AcFN$_2$H$_3$**, CD signals of L-**AcFTUNCS** at 268 and 300 nm are respectively attributed to phenyl thiourea and phenyl isothiocyanate chromophores, exhibiting characteristics similar to those of L,L-**AcFTU2**. This indicates an intramolecular chiral transfer in L-**AcFTUNCS** that is induced by the β-turn structure, agreeing with the solvent accessibilities probed by the solvent-dependent chemical shifts of the −NH protons and with the DFT optimized structure (Supplementary Fig. 13).

Supramolecular architectures

In view of the fact that the preferred heterochirality is accompanied by precipitation, we turn to the intermolecular packing of L,D- and L,L-**AcFTU2** in the molecules crystals. Heterochiral L,D-**AcFTU2** crystallizes in $P2_1/n$ space group, indicating a 2_1 screw axis, whereas homochiral L,L-**AcFTU2** crystallizes in $P1$ space group that indicates a sheet-like organization (Supplementary Table 2).

For clarity of showing the supramolecular network, the L-side with **β1**-turn in L,D-**AcFTU2** is depicted in blue, while D-side with **β1'**-turn in red, and the central benzene ring in gray (Fig. 4a). Interestingly, the intermolecular hydrogen bonds only occur between the sides of the same configuration of the phenylalanine residues (Fig. 4a), suggesting a high-fidelity of self-sorting dictates as homochiral self-sorting. Viewing from *b* axis, the L-sides of the L,D-**AcFTU2** molecules are bonded by head-to-tail N−H^a•••^{g}S=C and N−H^c•••^{f}O=C hydrogen bonds (Fig. 4a, b; for hydrogen bonding parameters, see Supplementary Table 4), leading to a supramolecular *M*-helix following a 2_1 screw axis of pitch 8.366 Å. Meanwhile, the D-sides form a *P*-helix that is a mirror-image of the *M*-helix formed from the L-sides (Fig. 4a). Therefore, within *bc* plane, L,D-**AcFTU2** molecules form a helix-array superstructure consisting of alternative *M*- and *P*-helices that are spaced by the central benzene rings (Supplementary Fig. 14), in which the helicity of β-turn could be well propagated.

Along *b* axis, parallel L,L-**AcFTU2** molecules are stacked by double N−H^c•••^{g}S=C hydrogen bonds between **β2** and **β3**-turns to form chains,

https://doi.org/10.1038/s41467-024-53744-x

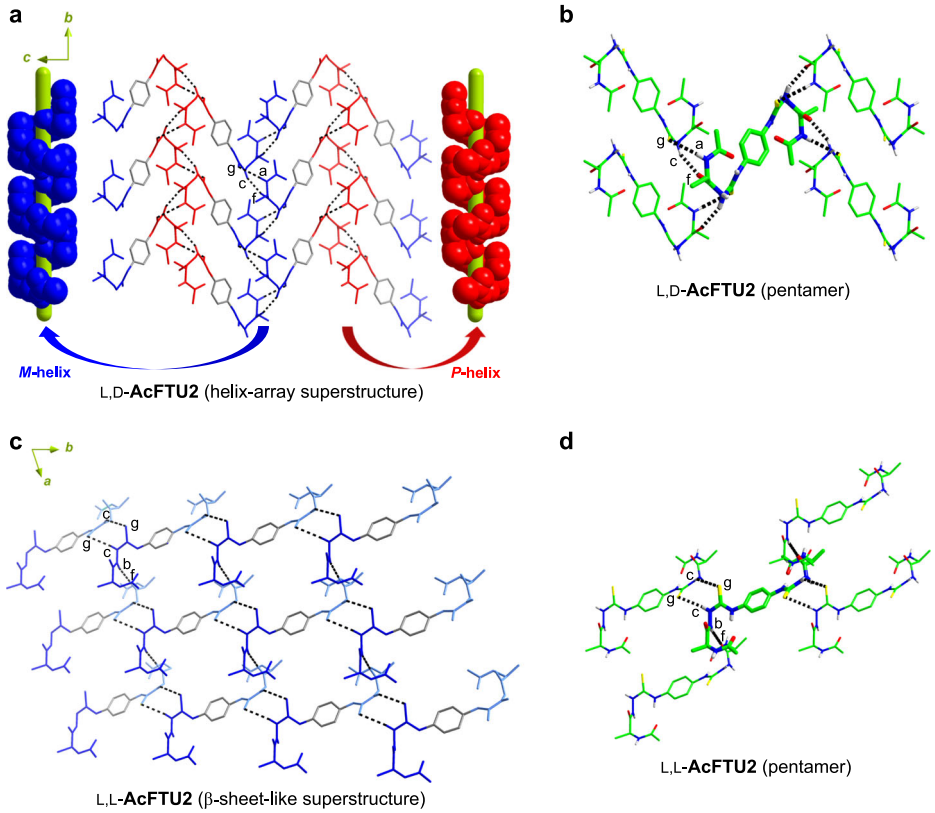

Fig. 4 | Supramolecular architectures of L,D-AcFTU2 and L,L-AcFTU2. a 2D helix-array superstructure of L,D-**AcFTU2** within *bc* plane, stacking via N–H^{a}•••^{g}S=C and N–H^{c}•••^{f}O=C hydrogen bonds, to lead in alternative *M*- and *P*-helices. The blue ones represent the sides of the molecule containing L-phenylalanine residues while red ones are the D-sides. **b** Hydrogen-bonded pentamer of L,D-**AcFTU2**. **c** 2D β-sheet-like superstructure of L,L-**AcFTU2** within *ab* plane, interacting via double N–H^{c}•••^{g}S=C hydrogen bonds along *b* axis and N–H^{b}•••^{f}O=C hydrogen bonds along *a* axis. Those highlighted in blue represent the sides with **β2**-turns while those in light blue with **β3**-turns. **d** Hydrogen-bonded pentamer of L,L-**AcFTU2**. Dashed black lines indicate intermolecular hydrogen bonds. For clarity, the hydrogen atoms that are not involved in the intermolecular hydrogen bonding and the benzene rings of phenylalanine residues are omitted.

which stack in a parallel manner along *a* axis via N–H^{b}•••^{f}O=C hydrogen bonds, resulting in a 2D superstructure similar to the biological β-sheet structure (Fig. 4c, d).

In the crystals each L,D-**AcFTU2** molecule interacts with four neighboring molecules via eight hydrogen bonds, while L,L-**AcFTU2** molecule interact with four neighboring ones via six hydrogen bonds, exhibiting significantly different hydrogen bonding networks in the pentamers (Fig. 4b, d). It is also noted that the L,D-**AcFTU2** molecule belongs to the C_i point group with zero dipole moment, whereas L,L-**AcFTU2** is of C_2 symmetry with a dipole moment along C_2 rotation axis. Computations show that the L,L-**AcFTU2** monomer has a dipole moment of 10.3 Debye (Supplementary Fig. 15). Since L,L-**AcFTU2** monomers are packed in the same orientation in the crystal, there would be significant electrostatic repulsion between the dipolar L,L-**AcFTU2** molecules that to some extent offsets the local hydrogen bonding. Such long range repulsion does not exist in the packing of L,D-**AcFTU2** molecule in the crystal. This dramatic difference in the crystal packings of L,D- and L,L-**AcFTU2** can be elucidated with quantum calculations of the binding of a monomer with its four surrounding monomers as described in the scheme of Supplementary Fig. 15, at M062X-D3/6-311 ++ G(d,p) level. Computational results demonstrated that the binding energy in the L,D-**AcFTU2** pentamer is 104 kcal/mol, higher than that of the L,L-**AcFTU2** pentamer (74.6 kcal/mol).

The difference in the intermolecular interactions in the homo- and heterochiral bilateral azapeptides can be further deduced from their solubilities. L,L-**AcFTU2** is much more soluble in MeCN than L,D-**AcFTU2** at the same temperature, for example, 60.5 μM for L,L-**AcFTU2** whereas 2.43 μM for L,D-**AcFTU2** at 25 °C (Supplementary Fig. 16). The increased solubility of L,L-**AcFTU2** with increasing temperature is more pronouncing than that of L,D-**AcFTU2**, leading to a larger difference in their solubilities at higher temperatures. Interestingly, both the heterochiral selectivity and the difference in the solubility of L,L- and L,D-**AcFTU2** in MeCN are positively temperature-dependent (Table 1 and Supplementary Fig. 16)[40]. A positive correlation is observed between the difference in solubilities ($s_{L,L}-s_{L,D}$) and the heterochiral selectivity in MeCN over the tested temperature range (Supplementary Fig. 17). Aggregation of diastereomers L,L- and L,D-**AcFTU2** in 95:5 (v/v) MeCN/DMSO mixtures also reveals distinct intermolecular interactions[41–45]. Fresh solution of L,D-**AcFTU2** at 2 mM, at which the NMR investigation on the intramolecular hydrogen bonding was carried out (Supplementary Fig. 8), exhibits polymeric species of diameter *ca*. 210 nm, as determined by dynamic light scattering (DLS) measurements (Supplementary Fig. 18). In addition, scanning electron microscopy (SEM) of an air-dried sample on a platinum-coated silicon wafer displays clustered rod-like aggregates (Supplementary Fig. 19). In contrast, DLS and SEM analyses of the L,L-**AcFTU2** sample show only monomeric components and amorphous solids. Aggregation of L,D-**AcFTU2** at lower concentration was further examined by DLS, which shows that it starts to form aggregates at 0.6 mM, of diameter *ca*. 60 nm (Supplementary Fig. 18). The fact that the chemical shifts of –NH protons in L,D-**AcFTU2** are close to those of L,L-**AcFTU2** (Supplementary Fig. 8) in CD_3CN/DMSO-d_6 mixtures of varying DMSO-d_6 composition (5–100% by volume) suggests that the NMR signals observed for L,D-**AcFTU2** are those from its monomeric species, since in all those

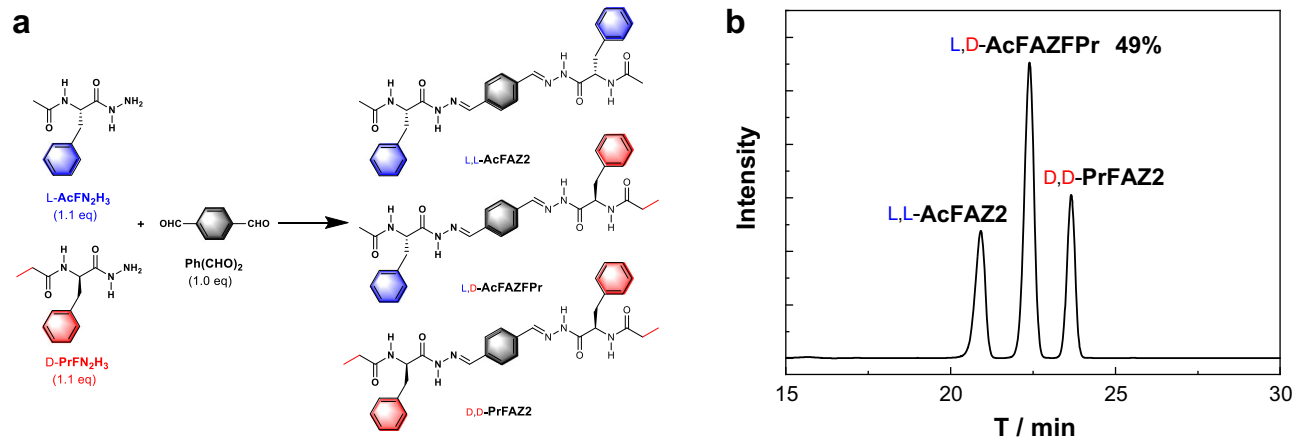

Fig. 5 | Reactions to bilateral acylhydrazones. a Reactions of L-$\mathbf{AcFN_2H_3}$ and D-$\mathbf{PrFN_2H_3}$ with $\mathbf{Ph(CHO)_2}$ to yield bilateral acylhydrazones. **b** HPLC traces of the products from the reaction of L-$\mathbf{AcFN_2H_3}$ and D-$\mathbf{PrFN_2H_3}$ with $\mathbf{Ph(CHO)_2}$. Experimental conditions: a solution of L-$\mathbf{AcFN_2H_3}$ (0.22 mmol), D-$\mathbf{PrFN_2H_3}$ (0.22 mmol), and $\mathbf{Ph(CHO)_2}$ (0.2 mmol) in a MeCN (10 mL) reacted in a high-pressure reactor at 100 °C for 24 h.

cases L,L-**AcFTU2** exists in the monomer form. This also prevents our detailed investigations by NMR of the intermolecular hydrogen bonding interactions between L,D-**AcFTU2** molecules in solution.

Thus, both computational binding energies, experimental solubilities, and aggregation behaviors in solutions reveal that the helical-like superstructure of heterochiral L,D-**AcFTU2** is more favorable than the β-sheet-like organization of homochiral L,L-**AcFTU2** molecule, accounting for the heterochiral coupling of bilateral azapeptides. A solid support for this conclusion is the disappearance of the diastereoselectivity in DMSO and DMF in which no aggregates exist (Table 1).

Bilateral acylhydrazones

The role of intramolecular helical β-turns for heterochiral coupling has not yet been demonstrated. We designed bilateral acylhydrazones that do not bear the β-turn structures. Replacing $\mathbf{Ph(NCS)_2}$ by $\mathbf{Ph(CHO)_2}$ (Fig. 5a), the reaction that yields bilateral acylhydrazones shows no heterochiral selectivity but random distribution, despite the formation of precipitation from the solutions (Fig. 5b and Supplementary Table 5). We, therefore, conclude that the β-turn structures contribute to the heterochirality during the formation of **AcFTU2**. It is the helical fragment that builds supramolecular helices from the heterochiral products, affording chiral architectures to induce diastereoselective couplings. Hence the observed heterochirality is the cooperative result of intramolecular hydrogen-bonded β-turns and intermolecular interactions, i.e., hydrogen bonding and dipole-dipole interactions.

Chiral amplification led by heterochirality

Amplification of a low *ee* (enantiomeric excess) has been considered a requisite for the origin of homochirality. It has been realized in a variety of experiments, such as crystallization[46], asymmetric autocatalysis[47], polymerization[48], sublimation[49], and adsorption[50]. Consider a sample of low *ee*, if its racemate portion is removed in the way of precipitation by reaction with an achiral reactant that prefers to forming a heterochiral product, the remaining starting material will be of higher *ee* and eventually homochiral (Fig. 6a)[11,51,52]. Therefore, our finding of the heterochiral preference may allow chiral amplification of the amino acid-based hydrazides (Fig. 6b, c).

Amplified *ee* of the $\mathbf{AcFN_2H_3}$ is indeed observed after treated with achiral $\mathbf{Ph(NCS)_2}$ and removal of the precipitates (Supplementary Table 6). Allow the reaction to take place in MeCN in a high-pressure reactor at 100 °C, *ee* of $\mathbf{AcFN_2H_3}$ increases only from 40% to 46% if 0.1 eq $\mathbf{Ph(NCS)_2}$ is added, with a further dramatic improvement to 82% or from −40% to −84% when 0.4 eq $\mathbf{Ph(NCS)_2}$ is loaded. However, at the lower temperature of 80 °C the *ee* increases only from 40% to 55% using 0.4 eq $\mathbf{Ph(NCS)_2}$, which is far less than that observed at 100 °C, likely due to the temperature-dependent strength of heterochirality (Table 1).

By adding 0.4 eq $\mathbf{Ph(NCS)_2}$, the amplification at 100 °C is not complete in one step, but with several cycles, the *ee* can be improved gradually from 20% to 93% or from −20% to −95% (Supplementary Table 7). Relating the *ee* before and after the reaction, an S-shaped curve is obtained (Fig. 6c, d), which looks similar to that observed in the classic chiral amplification termed the "majority rules effect"[53,54]. Compared with that of the reaction at 100 °C, chiral amplification at 80 °C decreases substantially (Supplementary Fig. 20). The observed chiral amplification again supports the heterochirality found in the reaction of racemate $\mathbf{AcFN_2H_3}$ with $\mathbf{Ph(NCS)_2}$.

Similar chiral amplification is also observed for the non-aromatic amino acid (alanine, valine) based hydrazides, $\mathbf{AcAN_2H_3}$ and $\mathbf{AcVN_2H_3}$, after treated with $\mathbf{Ph(NCS)_2}$ in MeCN (Fig. 6b–d), indicating that the preferred heterochirality could occur in the random reactions of these *N*-acylamino acid based hydrazides with $\mathbf{Ph(NCS)_2}$. According to this chiral amplification mechanism, the overall yield of the enantiomerically enriched substrates, i.e., $\mathbf{AcFN_2H_3}$, $\mathbf{AcAN_2H_3}$, and $\mathbf{AcVN_2H_3}$, is low because of the loss of most of the substrates in the formation of precipitate products (Fig. 6a, c). This loss is not advantageous for the preparation of enantiomerically pure substrates. Yet the chiral amplification mechanism remains significant in terms of understanding the origin of prebiotic homochirality, a compelling but challenging question.

Proline, a natural amino acid known to facilitate the formation of folded β-turn structures[35,55–57], is also explored in its hydrazide form, $\mathbf{AcPN_2H_3}$ (Fig. 6b). However, an almost linear relationship is observed for the *ee* before and after the reaction (Fig. 6d), indicating a substantially decreased or a lack of the heterochirality in the reaction of $\mathbf{AcPN_2H_3}$ with $\mathbf{Ph(NCS)_2}$. This absence can be attributed to the lack of the acetamido $-NH^a$ proton in the proline-based azapeptides (Fig. 6b), which would make it impossible to form favorable supramolecular architectures from the heterochiral products, for example the helix-array superstructures. Furthermore, when $\mathbf{Ph(CHO)_2}$ is used instead of $\mathbf{Ph(NCS)_2}$, the chiral amplification effect of the hydrazide substrates is not observed (Supplementary Table 8), due also to the observed absence of the heterochiral selectivity in the reactions of the bilateral acylhydrazones (Fig. 5).

Discussion

In summary, we report a heterochiral coupling to bilateral β-turn structured azapeptides, in which the two chiral centers are separated

https://doi.org/10.1038/s41467-024-53744-x

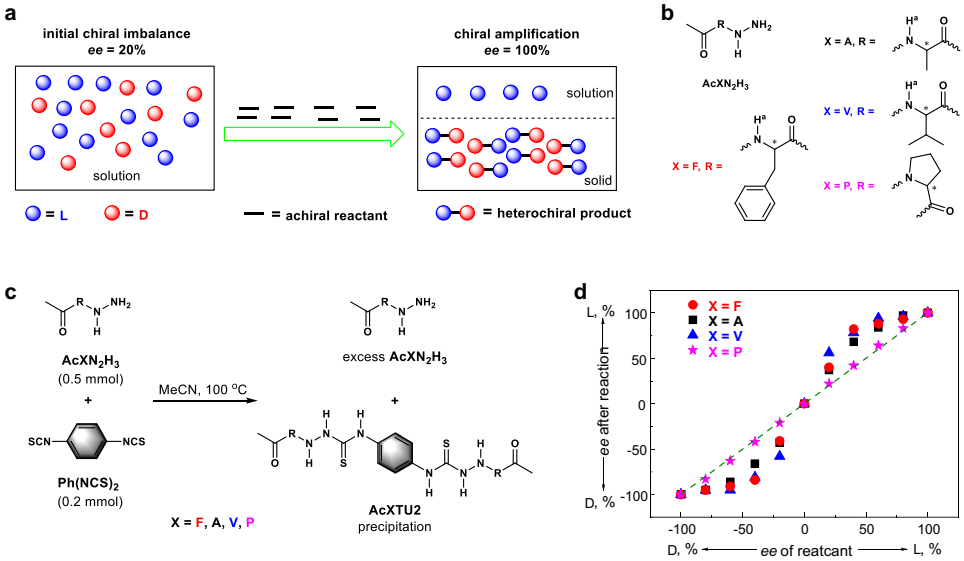

Fig. 6 | Chiral amplification of *N*-acylamino acid-based hydrazides via favored heterochirality. a Schematic diagram for chiral amplification led by heterochiral selectivity of bilateral reactions. **b** Structures of *N*-acylamino acid based hydrazides $\mathbf{AcXN_2H_3}$ (**X** = **F, A, V, P**). The asterisks in the structures indicate chiral carbons. **c** Reactions of excess $\mathbf{AcXN_2H_3}$ with $\mathbf{Ph(NCS)_2}$. Experimental conditions: a solution of $\mathbf{AcXN_2H_3}$ (0.5 mmol) of different *ee* and $\mathbf{Ph(NCS)_2}$ (0.2 mmol) in a high-pressure reactor in MeCN (10 mL) at 100 °C for 5 h. **d** *ee*s of $\mathbf{AcXN_2H_3}$ before and after its reaction with $\mathbf{Ph(NCS)_2}$.

by 14 atoms or 15 bonds. Notably, the central benzene ring linker breaks the intramolecular hydrogen bonding network and destroys the direct intramolecular asymmetric communication between the two remote chiral centers. However, a preference of heterochiral coupling was observed in the one-pot reaction of racemic *N*-acylphenylalanine based hydrazides with the achiral 1,4-di(isothiocyanine) benzene in MeCN that precipitates formed, yielding more heterochiral azapeptides than the homochiral counterparts. But in DMSO or DMF solutions no precipitates formed, and the couplings to bilateral azapeptides were essentially random. The solid-state aggregates of the heterochiral azapeptides feature a helical-like superstructure through intermolecular hydrogen bonding between homochiral β-turns, consisting of alternative *M*- and *P*-helices that allow the propagation of β-turn helicity. This helical-like superstructure is more favorable than the β-sheet-like superstructure of homochiral azapeptides, providing a mechanism for the favored heterochiral coupling of the one-pot reaction. Moreover, the heterochiral coupling leads to chiral amplification of hydrazides after being treated with a certain amount of the achiral reactant $\mathbf{Ph(NCS)_2}$, resulting in hydrazides of higher *ee* or enantiopurity. The present findings confirm the enantioselective synthesis induced by biomimetic supramolecular structures and provide a new avenue for the amplification of chirality.

Methods

General methods

^{1}H NMR and ^{13}C NMR spectra were obtained on a Bruker AV500 or AV600 spectrometer. Absorption spectra were recorded on a Thermo Scientific Evolution 300 UV/Vis spectrophotometer. CD spectra were recorded with a JASCO J-1500 spectropolarimeter. High-resolution mass spectra were obtained on a Bruker En Apex ultra 7.0 FT-MS. Infrared spectra were carried out using a Nicolet AVATAR FT-IR330 spectrometer. DLS was collected with a Malvern Zetasizer Nano-ZS90. SEM images were obtained on a ThermoFisher Helios 5 UC microscope. X-ray crystallography data of compounds L,D-**AcFTU2** and L,L-**AcFTU2** were collected on an Oxford Gemini S Ultra system. Absorption corrections were applied by using the program CrysAlis (multi-scan). The structure was solved by direct methods and non-hydrogen atoms except solvent molecules were refined anisotropically by least-squares on F^2 using the SHELXTL program. HPLC traces were recorded on Shimadzu Corporation LC-20AD chromatographic instrument with a UV detector and C18 or Chiralpak ID column.

Synthesis of the compounds

Detailed procedures for the synthesis of all compounds and their characterization data are given in the Supplementary Information.

Determination of diastereoselectivity by HPLC analysis

To determine the diastereoselectivity of the pseudo-racemic reaction system, the solvent was removed through vacuum distillation. 10 mg of the reaction product was dissolved in 0.5 mL DMSO, and then 50 μL of the resultant solution was transferred into 2 mL methanol to obtain a diluted sample. The sample was then analyzed using the following conditions: HPLC column C18 (250 × 4.6 mm), injection volume 10 μL, eluent methanol/water (50:50, v/v), flow 1 mL/min, room temperature, λ = 310 nm (azapeptides) or 330 nm (acylhydrazones). Retention times: L,L-**AcFTU2** 9.7 min, L,D-**AcFTUFPr** 13.2 min, D,D-**PrFTU2** 16.3 min; L,L-**AcFAZ2** 20.9 min, L,D-**AcFAZFPr** 22.4 min, D,D-**PrFAZ2** 23.6 min.

Determination of reaction rate constants

Compound L-intermediate (16.5 mg, 0.04 mmol) and L-$\mathbf{AcFN_2H_3}$ or D-$\mathbf{AcFN_2H_3}$ (8.84 mg, 0.04 mmol) were mixed in 20 mL MeCN and then stirred at different temperatures. Small portions of the reaction mixture were taken out at different reaction durations with quick filtrating, and 40 μL of the filtrate was added 1960 μL MeCN, and the resultant solution was subject to UV-Vis absorption measurements. The concentration of product (x) at reaction time (t) can be calculated based on absorption spectral measurements. The reaction rate constant k was obtained by fitting the integral form of the second-order reaction rate equation $kt = x/[c(c-x)]$.

Determination of solubility

Supersaturated solutions of L,L-**AcFTU2** or L,D-**AcFTU2** in MeCN were stirred at a certain temperature for several hours. The turbid solution was filtered to obtain saturated solutions of L,L-**AcFTU2** or L,D-**AcFTU2**. Then the saturated solutions were subjected to concentration determination by UV-Vis absorption spectra.

Determination of *ee* by chiral HPLC analysis

To determine the *ee* of **AcFN$_2$H$_3$**, **AcAN$_2$H$_3$**, and **AcVN$_2$H$_3$** after reactions, the precipitation was removed by filtration. The filtrate was then analyzed using the following conditions: HPLC column Chiralpak ID (250 × 4.6 mm), injection volume 10 μL, eluent *n*-hexane/2-propanol (75:25 for **AcFN$_2$H$_3$** and **AcAN$_2$H$_3$**, 80:20 for **AcVN$_2$H$_3$**, 65:35 for **AcPN$_2$H$_3$**, v/v), flow 1 mL/min, room temperature, λ = 220 nm. Retention times: L-**AcFN$_2$H$_3$** 33.1 min, D-**AcFN$_2$H$_3$** 17.0 min; L-**AcAN$_2$H$_3$** 20.5 min, D-**AcAN$_2$H$_3$** 13.1 min; L-**AcVN$_2$H$_3$** 21.7 min, D-**AcVN$_2$H$_3$** 13.1 min; L-**AcPN$_2$H$_3$** 36.5 min, D-**AcPN$_2$H$_3$** 23.1 min.

Data availability

The authors declare that all data supporting the findings of this study are available within the paper and its supplementary information files or available from the corresponding author upon request. The crystallographic data generated in this study have been deposited in the Cambridge Crystallographic Data Center with deposition numbers of CCDC 1586179 (L,D-**AcFTU2**) and 1586178 (L,L-**AcFTU2**). Source data are provided with this paper.

References

1. Ojima, I. Catalytic asymmetric synthesis. 3rd ed. Nashville (TN): John Wiley & Sons; (2013).
2. Silvi, M. & Melchiorre, P. Enhancing the potential of enantioselective organocatalysis with light. *Nature* **554**, 41–49 (2018).
3. Wendlandt, A. E., Vangal, P. & Jacobsen, E. N. Quaternary stereocentres via an enantioconvergent catalytic S_N1 reaction. *Nature* **556**, 447–451 (2018).
4. Li, M.-L., Yu, J.-H., Li, Y.-H., Zhu, S.-F. & Zhou, Q.-L. Highly enantioselective carbene insertion into N–H bonds of aliphatic amines. *Science* **366**, 990–994 (2019).
5. He, Y.-M. et al. Recent progress of asymmetric catalysis from a Chinese perspective. *CCS Chem.* **5**, 2685–2716 (2023).
6. Soai, K., Shibata, T., Morioka, H. & Choji, K. Asymmetric autocatalysis and amplification of enantiomeric excess of a chiral molecule. *Nature* **378**, 767–768 (1995).
7. Ruiz-Mirazo, K., Briones, C. & de la Escosura, A. Prebiotic systems chemistry: new perspectives for the origins of life. *Chem. Rev.* **114**, 285–366 (2013).
8. Brewer, A. & Davis, A. P. Chiral encoding may provide a simple solution to the origin of life. *Nat. Chem.* **6**, 569–574 (2013).
9. Birch, D., Hill, R. R., Jeffs, G. E. & North, M. Stereochemical preference for heterochiral coupling controls selectivity in competitive peptide synthesis. *Chem. Commun.* 941–942 (1999).
10. Hill, R. R., Birch, D., Jeffs, G. E. & North, M. Enantioselection in peptide bond formation. *Org. Biomol. Chem.* **1**, 965–972 (2003).
11. Deng, M., Yu, J. & Blackmond, D. G. Symmetry breaking and chiral amplification in prebiotic ligation reactions. *Nature* **626**, 1019–1024 (2024).
12. Crisma, M. et al. Meteoritic Cα-methylated α-amino acids and the homochirality of life: searching for a link. *Angew. Chem. Int. Ed.* **43**, 6695–6699 (2004).
13. Nery, J. G., Eliash, R., Bolbach, G., Weissbuch, I. & Lahav, M. Homochiral oligopeptides via surface recognition and enantiomeric cross impediment in the polymerization of racemic phenylalanine *N*-carboxyanhydride crystals suspended in water. *Chirality* **19**, 612–624 (2007).
14. Illos, R. A. et al. Oligopeptides and copeptides of homochiral sequence, via β-sheets, from mixtures of racemic α-amino acids, in a one-pot reaction in water; relevance to biochirogenesis. *J. Am. Chem. Soc.* **130**, 8651–8659 (2008).
15. Weissbuch, I., Illos, R. A., Bolbach, G. & Lahav, M. Racemic β-sheets as templates of relevance to the origin of homochirality of peptides: lessons from crystal chemistry. *Acc. Chem. Res.* **42**, 1128–1140 (2009).
16. Lee, D. H., Granja, J. R., Martinez, J. A., Severin, K. & Ghadiri, M. R. A self-replicating peptide. *Nature* **382**, 525–528 (1996).
17. Severin, K., Lee, D. H., Martinez, J. A. & Ghadiri, M. R. Peptide self-replication via template-directed ligation. *Chem. Eur. J.* **3**, 1017–1024 (1997).
18. Saghatelian, A., Yokobayashi, Y., Soltani, K. & Ghadiri, M. R. A chiroselective peptide replicator. *Nature* **409**, 797–801 (2001).
19. Budt, K. H., Vatele, J. M. & Kishi, Y. Terminal epoxidation of farnesate attached to helical peptides. *J. Am. Chem. Soc.* **108**, 6080–6082 (1986).
20. Linnane, P., Magnus, N. & Magnus, P. Induction of molecular asymmetry by a remote chiral group. *Nature* **385**, 799–801 (1997).
21. Tamai, Y. et al. Efficient 1,8- to 1,12-asymmetric induction in Grignard reactions of ω-keto esters by using BINOL or its 2′-oligoether derivatives as the chiral auxiliary. *J. Chem. Soc. Perkin Trans.* **1**, 1141–1142 (1999).
22. Kawasaki, T. et al. Point-to-point ultra-remote asymmetric control with flexible linker. *Chem. Eur. J.* **23**, 282–285 (2017).
23. Byrne, L., Sola, J. & Clayden, J. Screw sense alone can govern enantioselective extension of a helical peptide by kinetic resolution of a racemic amino acid. *Chem. Commun.* **51**, 10965–10968 (2015).
24. Tilly, D. P., McColl, C., Hu, M., Vitórica-Yrezábal, I. J. & Webb, S. J. Enantioselective conjugate addition to nitroolefins catalysed by helical peptides with a single remote stereogenic centre. *Org. Biomol. Chem.* **21**, 9562–9571 (2023).
25. Yan, X.-S. et al. β-Turn structure in glycinylphenylalanine dipeptide based *N*-amidothioureas. *Chem. Commun.* **49**, 8943–8945 (2013).
26. Zhang, Y. et al. Turn conformation of β-amino acid-based short peptides promoted by an amidothiourea moiety at C-terminus. *J. Org. Chem.* **85**, 9844–9849 (2020).
27. Cao, J. et al. C–I···π halogen bonding driven supramolecular helix of bilateral *N*-amidothioureas bearing β-turns. *J. Am. Chem. Soc.* **139**, 6605–6610 (2017).
28. Yan, X. et al. Single-handed supramolecular double helix of homochiral bis(*N*-amidothiourea) supported by double crossed C–I···S halogen bonds. *Nat. Commun.* **10**, 3610 (2019).
29. Shi, D. et al. Chalcogen bonding mediates the formation of supramolecular helices of azapeptides in crystals. *Org. Biomol. Chem.* **19**, 6397–6401 (2021).
30. Yan, X. et al. Solvophobic interaction promoted supramolecular helical assembly of building blocks of weak intermolecular halogen bonding. *Chem. Commun.* **57**, 1802–1805 (2021).
31. Yan, X., Weng, P., Shi, D. & Jiang, Y.-B. Supramolecular helices from helical building blocks via head-to-tail intermolecular interactions. *Chem. Commun.* **57**, 12562–12574 (2021).
32. Lin, X. et al. Spontaneous resolution of helical building blocks through the formation of homochiral helices in two dimensions. *Angew. Chem. Int. Ed.* **61**, e202205914 (2022).
33. Weng, P., Yan, X., Cao, J., Li, Z. & Jiang, Y.-B. Intramolecular chalcogen bonding to tune the molecular conformation of helical building blocks for a supramolecular helix. *Chem. Commun.* **58**, 6461–6464 (2022).
34. Sisco, S. W. & Moore, J. S. Homochiral self-sorting of BINOL macrocycles. *Chem. Sci.* **5**, 81–85 (2014).
35. Hutchinson, E. G. & Thornton, J. M. A revised set of potentials for β-turn formation in proteins. *Protein Sci.* **3**, 2207–2216 (1994).
36. Koch, O. Advances in the prediction of turn structures in peptides and proteins. *Mol. Inf.* **31**, 624–630 (2012).
37. Pescitelli, G., Di Bari, L. & Berova, N. Application of electronic circular dichroism in the study of supramolecular systems. *Chem. Soc. Rev.* **43**, 5211–5233 (2014).
38. Copeland, G. T., Jarvo, E. R. & Miller, S. J. Minimal acylase-like peptides. Conformational control of absolute stereospecificity. *J. Org. Chem.* **63**, 6784–6785 (1998).

39. Lee, H. J. et al. Role of azaamino acid residue in β-turn formation and stability in designed peptide. *J. Pept. Res.* **56**, 35–46 (2000).
40. Beaudoin, D., Rominger, F. & Mastalerz, M. Chiral self-sorting of [2+3] salicylimine cage compounds. *Angew. Chem. Int. Ed.* **56**, 1244–1248 (2017).
41. Yashima, E. et al. Supramolecular helical systems: helical assemblies of small molecules, foldamers, and polymers with chiral amplification and their functions. *Chem. Rev.* **116**, 13752–13990 (2016).
42. Wang, M. et al. Left or right: how does amino acid chirality affect the handedness of nanostructures self-assembled from short amphiphilic peptides? *J. Am. Chem. Soc.* **139**, 4185–4194 (2017).
43. Clover, T. M. et al. Self-assembly of block heterochiral peptides into helical tapes. *J. Am. Chem. Soc.* **142**, 19809–19813 (2020).
44. Wang, Y. et al. Self-templated, enantioselective assembly of an amyloid-like dipeptide into multifunctional hierarchical helical arrays. *ACS Nano* **15**, 9827–9840 (2021).
45. Bera, S., Umesh & Bhattacharya, S. Enhanced circularly polarized luminescence attained via self-assembly of heterochiral as opposed to homochiral dipeptides in water. *Chem. Sci.* **15**, 13987–13997 (2024).
46. Sogutoglu, L.-C., Steendam, R. R. E., Meekes, H., Vlieg, E. & Rutjes, F. P. J. T. Viedma ripening: a reliable crystallisation method to reach single chirality. *Chem. Soc. Rev.* **44**, 6723–6732 (2015).
47. Athavale, S. V., Simon, A., Houk, K. N. & Denmark, S. E. Structural contributions to autocatalysis and asymmetric amplification in the Soai reaction. *J. Am. Chem. Soc.* **142**, 18387–18406 (2020).
48. Yan, X., Wang, Q., Chen, X. & Jiang, Y.-B. Supramolecular chiral aggregates exhibiting nonlinear CD–*ee* dependence. *Adv. Mater.* **32**, 1905667 (2020).
49. Perry, R. H., Chunping, W., Nefliu, M. & Cooks, R. G. Serine sublimes with spontaneous chiral amplification. *Chem. Commun.* **14**, 1071–1073 (2007).
50. Yun, Y. & Gellman, A. J. Adsorption-induced auto-amplification of enantiomeric excess on an achiral surface. *Nat. Chem.* **7**, 520–525 (2015).
51. Breslow, R. & Levine, M. S. Amplification of enantiomeric concentrations under credible prebiotic conditions. *Proc. Natl Acad. Sci. USA* **103**, 12979–12980 (2006).
52. Ueda, M. et al. Alternating heterochiral supramolecular copolymerization. *J. Am. Chem. Soc.* **143**, 5121–5126 (2021).
53. Green, M. M. et al. Majority rules in the co-polymerization of mirror image isomers. *J. Am. Chem. Soc.* **117**, 4181–4182 (1995).
54. Palmans, A. R. A. & Meijer, E. W. Amplification of chirality in dynamic supramolecular aggregates. *Angew. Chem. Int. Ed.* **46**, 8948–8968 (2007).
55. Bomar, M. G., Song, B., Kibler, P., Kodukula, K. & Galande, A. K. An enhanced β turn in water. *Org. Lett.* **13**, 5878–5881 (2011).
56. Chung, M.-K., White, P. S., Lee, S. J., Gagné, M. R. & Waters, M. L. Investigation of a catenane with a responsive noncovalent network: mimicking long-range responses in proteins. *J. Am. Chem. Soc.* **138**, 13344–13352 (2016).
57. Metrano, A. J. et al. Diversity of secondary structure in catalytic peptides with β-turn-biased sequences. *J. Am. Chem. Soc.* **139**, 492–516 (2017).

Acknowledgements

This work has been supported by the National Science Foundation of China (21820102006, 22241503 and 92356308, Y.-B.J., 22101240, X.Y.), the Fundamental Research Funds for the Central Universities (20720220005, Y.-B.J., 20720220121, X.Y.) and the Natural Science Foundation of Fujian Province of China (2023J01038, X.Y.).

Author contributions

Y.-B.J. conceived the concept. X.Y. and Y.-B.J. designed the experiments and analyzed the data. X.Y. and J.C. performed the experiments. H.L. synthesized alanine- and valine-based hydrazides. Z.C. and Y.M. helped with DFT calculations. Z.L. contributed to the discussions. X.Y. wrote the manuscript with contributions from all authors.

Competing interests

The authors declare no competing interests.

Additional information

Supplementary information The online version contains supplementary material available at https://doi.org/10.1038/s41467-024-53744-x.

Correspondence and requests for materials should be addressed to Yun-Bao Jiang.

Peer review information *Nature Communications* thanks the anonymous reviewer(s) for their contribution to the peer review of this work. A peer review file is available.